Linewidth narrowing and Purcell enhancement in photonic crystal cavities on an Er-doped silicon nitride platform

Yiyang Gong*[1], Maria Makarova*[1], Selçuk Yerci[2], Rui Li[2], Martin J. Stevens[4], Burm Baek[4], Sae Woo Nam[4], Robert H. Hadfield[5], Sander N. Dorenbos[6], Val Zwiller[6], Jelena Vučković[1], and Luca Dal Negro[2,3]

[1] *Department of Electrical Engineering, Stanford University, Stanford, CA 94305*
[2] *Department of Electrical and Computer Engineering and Photonics Center, Boston University, Boston, MA 02215*
[3] *Division of Material Science and Engineering, Boston University, Boston, MA 02215*
[4] *National Institute of Standards and Technology, 325 Broadway, Boulder, CO*
[5] *School of Engineering and Physical Sciences, Heriot-Watt University, Edinburgh, EH14 4AS, United Kingdom*
[6] *Quantum Transport, Kavli Institute of Nanoscience, TU Delft 2628CJ Delft, The Netherlands*
[*] *These authors contributed equally to this work*

yiyangg@stanford.edu

Abstract: Light emission at 1.54 μm from an Er-doped amorphous silicon nitride layer coupled to photonic crystal resonators at cryogenic and room temperatures and under varying optical pump powers has been studied. The results demonstrate that small mode volume, high quality factor resonators enhance Er absorption and emission rates at the cavity resonance. Time resolved measurements give 11- to 17-fold Purcell enhancement of spontaneous emission at cryogenic temperatures, and 2.4-fold enhancement at room temperature. Resonances exhibit linewidth narrowing with pump power, signifying absorption bleaching and partial inversion of the Er ions cryogenic temperatures. We estimate that 31% of Er ions are excited at the highest pump power.

OCIS codes: (230.5298) Photonic crystals; (230.5750) Resonators; (230.6080) Sources; (260.3800) Luminescence; (160.5690) Rare-earth doped materials; (300.0300) Spectroscopy.

References and links

1. L. Pavesi, "A review of the various approaches to a silicon laser," Proc. SPIE **4997**, 206 (2003).
2. S. Yerci, R. Li, S. O. Kucheyev, T. van Buuren, S. N. Basu, and L. Dal Negro. "Energy transfer and 1.54 μm emission in amorphous silicon nitride films," Appl. Phys. Lett. **95**, 031107 (2009).
3. R. Li, S. Yerci, and L. Dal Negro "Temperature dependence of the energy transfer from amorphous silicon nitride to Er ions," Appl. Phys. Lett. **95**, 041111 (2009).
4. W. C. Ding, D. Hu, J. Zheng, P. Chen, B. W. Cheng, J. Z. Yu and Q. M. Wang. "Strong visible and infrared photoluminescence from Er-implanted silicon nitride films," J. Phys. D: Appl. **41**, 135101 (2008).
5. J. Warga, R. Li, S. N. Basu, and L. Dal Negro, "Electroluminescence from silicon-rich nitride/silicon superlattice structures," Appl. Phys. Lett. **93**, 151116 (2008).
6. E. M. Purcell, "Spontaneous emission probabilities at radio frequencies," Phys. Rev. **69**, 681 (1946).
7. O. Painter, R. K. Lee, A. Scherer, A. Yariv, J. D. O'Brien, P.D. Dapkus, and I. Kim, "Two-Dimensional Photonic Band-Gap Defect Mode Laser," Science **284**, 1819-1821 (1999).
8. M. Lončar, T. Yoshie, A. Scherer, P. Gogna, and Y. Qiu, "Low-threshold photonic crystal laser," Appl. Phys. Lett. **81**, 2680-2682 (2002).

#120921 - $15.00 USDReceived 3 Dec 2009; revised 12 Jan 2010; accepted 15 Jan 2010; published 25 Jan 2010

9. M. Makarova, V. Sih, J. Warga, R. Li, L. Dal Negro, J. Vučković, "Enhanced light emission in photonic crystal nanocavities with Erbium-doped silicon nanocrystals," Appl. Phys. Lett. **92**, 161107 (2008).
10. Y. Akahane, T. Asano, B-S. Song and S. Noda, "High-Q photonic nanocavity in a two-dimensional photonic crystal," Nature **425**, 944 (2003).
11. Dirk Englund, Ilya Fushman, and J. Vučković, "General recipe for designing photonic crystal cavities," Opt. Express, **13**, 5961 (2005).
12. R. Li, J. R. Schneck, J. Warga, L. D. Ziegler, and L. Dal Negro, "Carrier dynamics and erbium sensitization in silicon-rich nitride nanocrystals," Appl. Phys. Lett. **93**, 091119 (2008).
13. M. Makarova, Y. Gong, S-L. Cheng, Y. Nishi, S. Yerci, R. Li, L. Dal Negro, J. Vučković. "Photonic Crystal and Plasmonic Silicon Based Light Sources," accepted by JSTQE (2009).
14. E. Desurvire, *Erbium-doped fiber amplifiers: principles and applications*, pp. 230-253. John Wiley & Sons: New York, 1994.
15. R. H. Hadfield, M. J. Stevens, S. G. Gruber, A. J. Miller, R. E. Schwall, R. P. Mirin and S. W. Nam, "Single photon source characterization with a superconducting single photon detector," Opt. Express **13**, 10846 (2005).
16. G. N. Gol'tsman, O. Okunev, G. Chulkova, A. Lipatov, A. Semenov, K. Smirnov, B. Voronov, A. Dzardanov, C. Williams and R. Sobolewski, "Picosecond superconducting single-photon optical detector," Appl. Phys. Lett. **79**, 705 (2001).
17. K. M. Rosfjord, J. K. W. Yang, E. A. Dauler, A. J. Kerman, V. Anant, B. M. Voronov, G. N. Gol'tsman and K. K. Berggren, "Nanowire Single-photon detector with an integrated optical cavity and anti-reflection coating," Opt. Express **14**, 527 (2006).
18. E. A. Dauler, A. J. Kerman, B. S. Robinson, J. K. W. Yang, B. Voronov, G. Gol'tsman, S. A. Hamilton and K. K. Berggren, "Photon-number-resolution with sub-30-ps timing using multi-element superconducting nanowire single photon detectors," J. Mod. Opt. **56**, 364-373 (2009).
19. S.N. Dorenbos, E. M. Reiger, U. Perinetti, V. Zwiller, T. Zijlstra, T. M. Klapwijk, "Low noise superconducting single photon detectors on silicon," Appl. Phys. Lett. **93**, 131101 (2008).
20. M. T. Tanner, C. M. Natarajan, V. K. Pottapenjara, J. A. O'Connor, R. J. Warburton, R. H. Hadfield. B. Baek, S. Nam, S. N. Dorenbos, T. Zijlstra, T. M. Klapwijk, V. Zwiller, "Enhanced telecom wavelength sensitivity in NbTiN superconducting nanowire single-photon detectors fabricated on oxidized silicon substrates," Proceedings of Single Photon Workshop 2009 (Boulder, Colorado, 2009).
21. W. Becker, *Advanced Time-Correlated Single Photon Counting Techniques* (Springer Series in Chemical Physics, Vol. 81, 2005).
22. B. Henderson, G. F. Imbusch. *Optical Spectoscopy of Inorganic Solids*. Oxford University Press: New York, 1989.
23. A. Polman, D. C. Jacobson, D. J. Eaglesham, R. C. Kistler, and J. M. Poate, "Optical doping of waveguide materials by MeV Er implantation," J. Appl. Phys. **70**, 3778 (1991).
24. H. J. Kimble, "Structure and dynamics in cavity quantum electrodynamics," in *Cavity Quantum Electrodynamics*, edited by P. Berman, pp. 203-267, Academic Press, 1994.
25. L. A. Coldren, S. W. Corzine, *Diode Lasers and Photonic Integrated Circuits*, pp. 226-227. John Wiley & Sons: New York, 1995.

1. Introduction

There is a large effort to fabricate a laser with Si-complementary metal-oxide-semiconductor (CMOS) compatible processing technology, enabling monolithic integration with electronic components while keeping the production cost low [1]. One especially attractive material for this application is Er-doped amorphous silicon nitride (Er:SiN_x), which emits at the telecom wavelength of 1.54 μm [2, 3, 4]. The Er emission can be sensitized by the host through a nanosecond-fast energy transfer mechanism from the amorphous nitride matrix (SiN_x), which provides four orders of magnitude larger excitation cross-section than Er in silica (SiO_2) [2, 3]. Furthermore, it may be possible to electrically excite Er ions in this host, as indicated by initial work on electroluminescence of silicon nano-crystals in silicon-silicon nitride superlattices [5].

In this paper, we study emission from (Er:SiN_x) coupled to photonic crystal (PC) resonators with small mode volumes (V_{mode}) and high quality (Q)-factors to simultaneously maximize the Er-cavity mode coupling and the density of optical modes. This leads to an enhanced spontaneous emission rate into the cavity mode through the Purcell effect ($\propto Q/V_{mode}$) [6] and redirection of the majority of spontaneously emitted photons into the single mode. The corresponding increase in the spontaneous emission coupling factor β can be used to lower the lasing threshold [7, 8]. We have already demonstrated enhancement of Er photoluminescence (PL) in Si-rich

#120921 - $15.00 USDReceived 3 Dec 2009; revised 12 Jan 2010; accepted 15 Jan 2010; published 25 Jan 2010

Silicon Nitride (SRN) PC cavities in the presence of Si nanocrystals [9]. Here, we report on the observation of linewidth narrowing enabled by improved cavity Q/V_{mode}-factors and superior material properties that lead to increased PL efficiency and decreased non-radiative relaxation. These results indicate that it may be possible to achieve gain and lasing in the Er:SiN_x material.

We also confirm that small mode volume cavities are essential for observation of linewidth narrowing by looking at behavior of larger micro-ring resonators with similar Q-factors made in the same material system. The results support the theoretical expectation that material absorption rates are enhanced in a small mode volume, high-Q resonator, similar to Purcell enhancement of spontaneous emission. From time resolved measurements, we find that the average Purcell enhancement of spontaneous emission is 11 to 17 times in our PC resonators at cryogenic temperatures, and 2.4 times at room temperature.

2. Resonator fabrication and design

2.1. Material and Resonator fabrication

Er:SiN_x is grown on top of a Silicon on Insulator (SOI) wafer by N_2 reactive magnetron co-sputtering from Si and Er targets in a Denton Discovery 18 confocal-target sputtering system, as discussed elsewhere [2]. The growth is followed by a post-annealing process in a rapid thermal annealing furnace at 1170°C for 340 s under forming gas (5% H_2, 95% N_2) atmosphere. The Er concentration was measured as $3.0 \times 10^{20}\text{cm}^{-3}$ [2, 3].The fabrication of the resonators employs electron beam lithography with 350 nm of ZEP-520A as the resist. The written pattern is then etched into the Er:SiN_x (index of refraction $n_{Er} = 2.0$) and Si ($n_{Si} = 3.5$) slab with a HBr:Cl_2 chemistry. Finally, suspended PC membranes can be formed by undercutting with a 6:1 buffered oxide etch. PC and micro-ring structures fabricated in a 359 nm-thick hybrid 113-nm-Er:SiN_x/246-nm-Si membrane are shown in Figure 1(a),(c) with a scanning electron microscope (SEM).

2.2. Cavity design

Two dimensional (2D) PC cavities and micro-ring cavities are designed and optimized with three dimensional finite difference time domain (FDTD) simulations. For the PC cavity, we assume the period a=410 nm, the total slab thickness t=0.88a, the Er:SiN_x layer thickness t_{Er}=t/3, and the hole radius $r = 0.3a$. We employ the L3 photonic crystal cavity design [10, 11] with a transverse-electric (TE)-like mode, and maximize cavity Q-factor. For this membrane design, the Q-factor is maximized for a cavity with the end holes of the cavity laterally shifted out by 0.20a and having radius $r = 0.25a$, with the second level end holes shifted out by 0.10a (Figure 1a). The optimized cavity design has normalized frequency a/λ = 0.26, simulated quality factor $Q = 32,000$, and mode volume $V_{mode} = 0.85(\lambda/n)^3$ for a reference refractive index of n=3.5. The electric field magnitude at the middle of the membrane ($|\vec{E}|^2$) is shown in Figure 1(b). The overlap of optical mode with the Er:SiN_x layer, defined as the ratio of electric field energy in the active material to the energy in the whole resonator, is 4%.

Micro-ring resonators with a radius of 10μm are also designed with the same hybrid membrane. In order to enhance PL collection from the ring, a ridge waveguide is coupled to the ring resonator and PL directed to a scattering grating out-coupler at the end of the waveguide 1(c). The gap between the ring and waveguide is approximately 300 nm, and is well controlled by skipping the undercut step in fabrication. In the FDTD simulation, the fundamental TE whispering gallery mode (WGM) of the ring resonator at 1530 nm corresponds to an azimuthal number of $m = 60$ (Fig 1(d)), and has $Q = 15,000$ and $V_{mode} = 14(\lambda/n)^3$, where n is the index of Si. Nearby modes have similar Qs above 10,000. The mode has an overlap of 4% with the active material, similar to the PC cavity mode. The free spectral range of the fundamental TE

#120921 - $15.00 USDReceived 3 Dec 2009; revised 12 Jan 2010; accepted 15 Jan 2010; published 25 Jan 2010

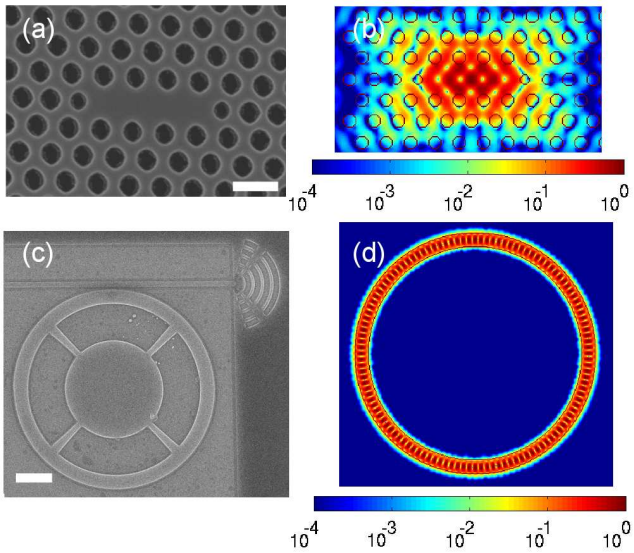

Fig. 1. (a) SEM picture of the fabricated PC cavity. The nearest end holes of the PC are shifted out by $0.20a$, and the second nearest end holes are shifted out by $0.10a$. The marker denotes 600 nm. (b) Electric field pattern ($|E|^2$) of the PC cavity mode. (c) SEM picture of the fabricated micro-ring structure with radius of 10 μm and the out-coupling waveguide and grating. Marker represents 4 μm. (d) Electric field pattern ($|E|^2$) of azimuthal number $m = 60$ micro-ring mode.

mode is expected to be 8nm, and the overlap parameter is expected to be approximately the same for all fundamental TE modes.

3. Optical measurements

3.1. Set-up for optical measurements

The optical experiments are conducted by pumping the cavity structures at normal incidence with a diode laser through a 100X objective with numerical aperture NA=0.5, and collecting the emission around 1530 nm through the same objective. Spectra are acquired by a 750 mm monochromator with 800 grooves/mm grating and a cryogenically cooled InGaAs linear CCD with $25 \times 500 \mu m$ pixels. A liquid helium flow cryostat is used to study samples at varying temperatures from 3.1K to room temperature.

We can excite Er non-resonantly by pumping the Er:SiN_x matrix at λ=400 nm or resonantly by pumping the $I_{15/2} \rightarrow I_{11/2}$ transition of erbium at λ=980 nm. While the 400 nm excitation takes advantage of the SiN_x-enhanced excitation cross-section, the Si part of the PC membrane strongly absorbs 400 nm excitation, generating undesirable free carriers and causing absorptive losses at the cavity resonance [2, 12]. In the future, it may be possible to take advantage of the larger excitation cross-section at 400 nm without suffering free-carrier absorption losses by eliminating Si from the resonator design. To minimize free-carrier absorption effects, we use 980 nm excitation to study gain in the Er-doped SiN_x film. Using 980 nm excitation, we observe an order of magnitude increase in the maximum cavity PL intensity relative to 400 nm excitation in PC resonators [13]. This observation confirms the expectation of lower absorptive losses in the silicon portion of the membrane under 980nm pumping. Fig. 2(b) shows PL from the unpatterned Er:SiN_x film at room and cryogenic temperatures pumped at 980 nm. The

#120921 - $15.00 USDReceived 3 Dec 2009; revised 12 Jan 2010; accepted 15 Jan 2010; published 25 Jan 2010

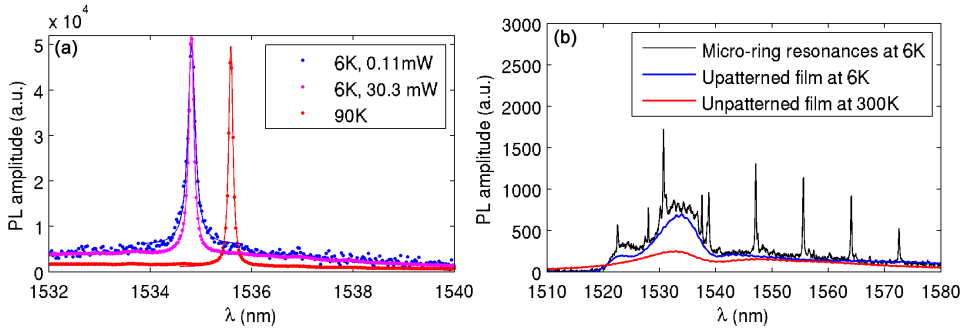

Fig. 2. (a) Normalized spectra of PC cavities at temperatures of 6 K (magenta, blue) and 90 K (red). For 6 K the spectra taken at low pump power of 0.11 mW (blue) and high pump power of 30.3 mW (magenta) are shown, demonstrating line-width narrowing with increasing pump power. The solid lines are Lorentzian fits used to determine cavity Qs (9,000 at 0.11 mW-pump at 6K, 13,300 at 30.3 mW at 6K, and 16,000 at 90K). (b) Micro-ring resonances at 6K (black), and spectra of Er emission from unpatterned film at room (red) and cryogenic (blue) temperatures.

maximum achievable power from the 980 nm pump laser was 35 mW in this setup.

The pump spot has an approximately 2 μm radius for all measurements. Thus, for PC cavities measurements, the pump beam covers the entire resonator and a portion of PC mirror. For micro-ring measurements, the pump beam is placed at the edge of the micro-ring on the side opposite the out-coupling waveguide, and PL is collected through the waveguide and out-coupling grating. Spectra of PC and micro-ring resonators are shown in Figure 2(a) and (b), respectively. Typical Qs of both systems are above 10,000.

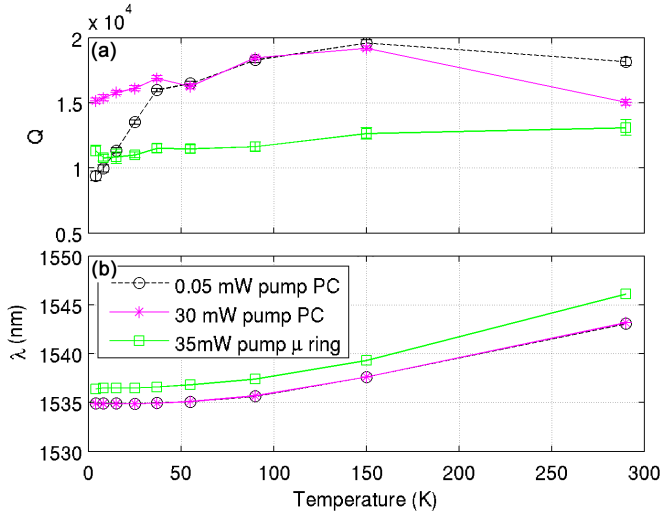

Fig. 3. Temperature dependence of (a) cavity Q-factor and (b) cavity resonance wavelength measured at 0.050 mW pump power and 30mW pump power for the PC cavity, and also for a micro-ring cavity mode at 35mW.

#120921 - $15.00 USDReceived 3 Dec 2009; revised 12 Jan 2010; accepted 15 Jan 2010; published 25 Jan 2010

3.2. *Photonic crystal resonators under varying pump power and temperature*

The temperature dependence of cavity resonance wavelength and Q-factor for the PC cavity are shown in Figure 3. The data are taken both at low (0.050 mW) pump power and high (30 mW) pump power. The resonance position red-shifts as the sample temperature is increased due to the slight increase in refractive index of Si with temperature. Moreover, the PC cavity Q measured at low pump power decreases from its room-temperature value as the cavity is cooled to 6 K. However, the Q-factor returns to a higher value when the cavity is pumped with high power at low temperatures. The PC cavity wavelength does not shift significantly between the low and high pump power conditions, as seen in the Figure 3(b). Thus, the observed increase in Q with increasing pump power at low temperature is attributed to the reduction of cavity losses, instead of to changes in the cavity refractive index (e.g. by heating).

The power dependence of the integrated cavity PL intensity and Q-factor are plotted in Figure 4(a) and (b), respectively, for a single cavity at temperatures of 6 K and 90 K. The cavity PL amplitude increases sub-linearly at both temperatures as seen in Figure 4(a). The cavity Q-dependence on pump power is drastically different at 6 K and 90 K. At 90 K the Q-factor maintains its value of 16,000 as the pump power is varied from 0.020 mW to 30 mW. At 6 K, the Q-factor increases gradually from 9,000 at low pump power to 13,300 at 30 mW pump power.

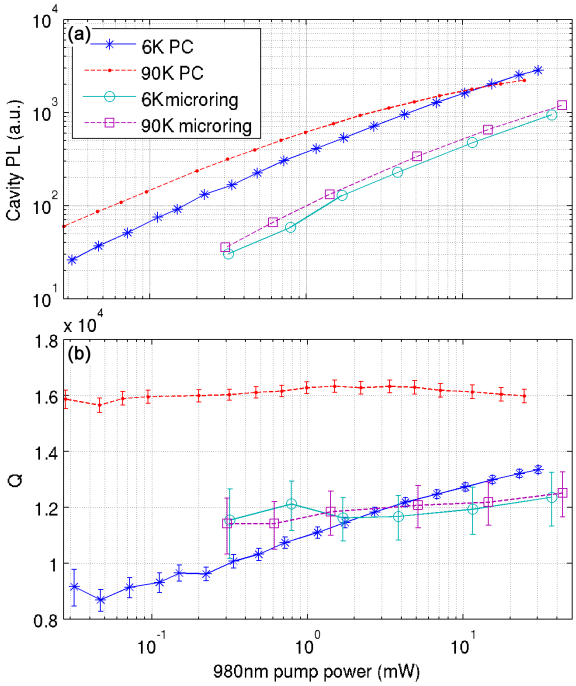

Fig. 4. Pump power dependence of (a) the integrated cavity intensity and (b) the cavity Q for PC and micro-ring cavity modes at different temperatures.

We repeat the temperature and power variation studies for a variety of PC cavities with wavelengths spanning the Er-emission spectrum from 1525 nm to 1560 nm. By tuning the radius of the holes in the photonic crystal within $\pm 1\%$ on either side of the mean, cavities are fabricated with a range of operating wavelengths. The characterized cavities are expected to have approximately the same intrinsic or cold cavity Q, as they are fabricated on the same chip with the

#120921 - $15.00 USDReceived 3 Dec 2009; revised 12 Jan 2010; accepted 15 Jan 2010; published 25 Jan 2010

same design. In Fig. 5(a), each line traces the low pump-power ($< 10\mu$W) Q vs. wavelength for an individual cavity as the sample temperature is gradually increased from 6 K to 290 K. The points along each line are taken at the same intermediate temperatures as in Fig. 3(a) for the PC cavity. The Er emission from the unpatterned film is also shown for reference. The cavities that overlap the main Er emission peak at 1535 nm and on the short wavelength side of the emission peak clearly demonstrate a large decrease in Q as the temperature is decreased. In fact, this wavelength range (from 1525 nm to 1540 nm) corresponds to the absorption peak of Er [14]. Note that room temperature Qs are high irrespective of where the cavities couple spectrally to the Er emission. Therefore, it appears that Q drops at cryogenic temperatures because the Er ion absorption increases at cryogenic temperatures. Figure 5(b) shows the difference in Q between the low pump power and high pump power measurements for each cavity as the sample temperature is raised. The maximum increase in Q-factor with pump power occurs at the lowest temperature (6K). On the other hand, at room temperature the cavity Q-factor drops at high pump power as a result of absorptive losses due to heating in the Si-portion of PC membrane. The decrease in Q becomes more apparent for the cavities at longer wavelengths.

3.3. Micro-ring resonators under varying pump power and temperature

We attempt the same temperature and pump-power dependence measurements for larger mode volume micro-ring cavities. As noted above, such cavities support WGMs that also have high Q, but have over an order of magnitude higher mode volume than the PC cavity modes. Because the ring cavities are 10 μm in radius, which is much larger than the pump spot size (2 μm radius), we pump only one section of the ring. We take the power series of a WGM well coupled to the Er main peak, for both 6K and 90K, shown in Fig. 4(a)-(b). The WGM modes typically have Qs of over 10,000, and multiple azimuthal numbers of the fundamental TE modes can be measured for the same ring cavity. The integrated cavity emission shows a sublinear increase with increasing pump power, while the cavity Q remains the same within the error of the measurement for all pump powers for both temperatures. The latter result is expected, as only a small section of the ring is pumped, and the lossy mechanisms of the entire ring are not significantly changed with pump power. In this case, the Q factor measured at high pump power is a good representation of the Q-factor at low pump power. In addition, the cavity resonance wavelength exhibits the same temperature dependence as the PC cavities, experiencing a small shift up from 6 K to 90 K, and having a large shift for higher temperatures (Fig. 3(b)).

In contrast to PC cavities, we observe that the Q for the micro-ring cavities increases by only 1,500 between 6 K and room temperature at high pump power, shown in Fig. 3(a). Since we pump only one section of the ring, we compare these results to the PC cavity Qs at low pump power. In fact, we observe that the change in Q of WGM for varying temperatures is far less than that of PC cavity modes. We also observe the change in Q as a function of the temperature for multiple cavity modes throughout the Er emission spectrum, all measured at high pump power, plotted in Fig. 5(c) with each line representing a cavity mode as temperature is increased. Cavities coupled to the Er main emission peak experience an increase of at most 2,000 in Q as the temperature is increased from 6K to room temperature, much less than $\Delta Q = 6,300$ of the PC cavities. However, cavities that are detuned from the main Er emission peak experience a smaller increase in Q or even a decrease in Q as the temperature is increased.

4. Spontaneous emission rate enhancement in PC cavities

Time resolved PL measurements are performed using a similar setup as for spectral measurements, but with a lower resolution grating of 300 grooves/mm and with the spectrometer output directed through a slit. The resulting spectrally filtered PL is coupled into a single-mode fiber and directed to a superconducting nanowire single-photon detector (SNSPD), which is held at

#120921 - $15.00 USDReceived 3 Dec 2009; revised 12 Jan 2010; accepted 15 Jan 2010; published 25 Jan 2010

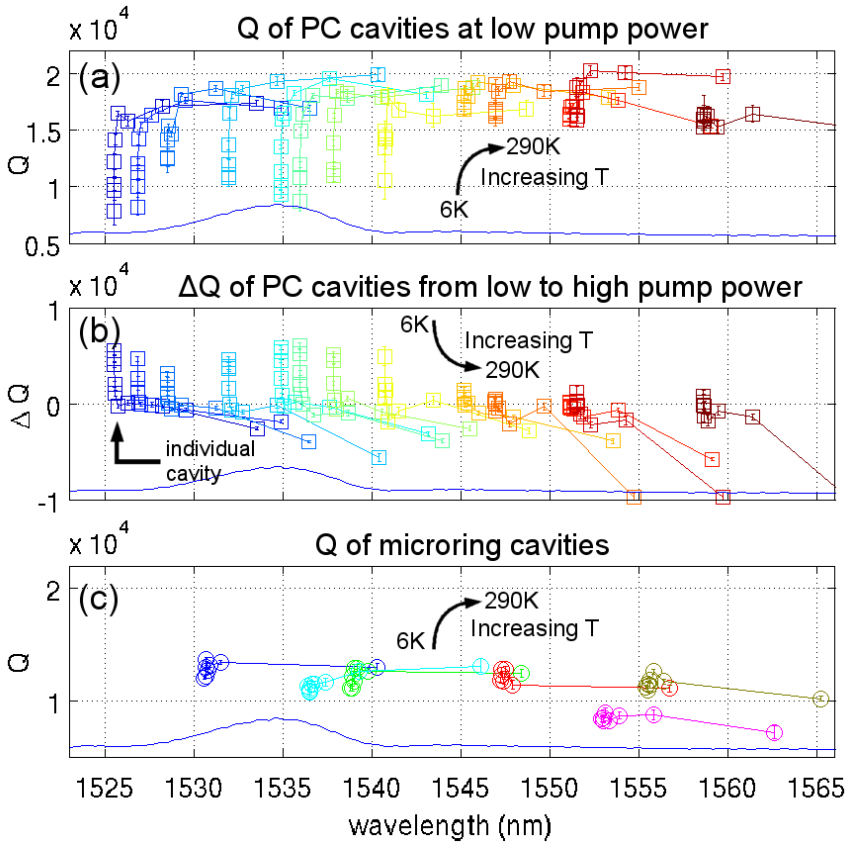

Fig. 5. (a) *Q*s for a number of PC cavities at low pump power as temperature is increased from 6 K to 290 K. Different colors show the wavelengths and *Q*s of individual cavities with varying temperature. The points along each line are taken at the same intermediate temperatures as in Fig. 3(a) for the PC cavity. (b) Change in *Q* as the pump power is switched from 0.050 mW to 30 mW for a number of PC cavities measured at temperatures from 6 K to 290 K. (c) *Q* for micro-ring cavities as temperature is increased from 6 K to 290 K. The points along each line are taken at the same intermediate temperatures as in Fig. 3(a) for the micro-ring cavity.

#120921 - $15.00 USDReceived 3 Dec 2009; revised 12 Jan 2010; accepted 15 Jan 2010; published 25 Jan 2010

a temperature of 3K in a closed-cycle helium cryocooler [15]. SNSPDs are sensitive to photons over a broad spectral range spanning from the ultraviolet to the near-infrared and have been demonstrated to achieve very low timing jitter (<30 ps) and high detection efficiency (>50%) [15, 16, 17, 18]. The SNSPD used here consists of a 100 nm-wide, current-biased superconducting NbTiN wire meandering over a 10×10 μm^2 area. A fraction of the wire is driven into a resistive state and delivers an output voltage pulse upon absorption of one photon [16]. The wire is deposited on an oxidized Si substrate (225 nm SiO_2 thickness). Reflections at the SiO_2/Si interface lead to an enhanced efficiency of 13% at λ = 1300 nm, with up to ≈5% efficiency at 1550 nm at a dark count rate of ≈ 100 Hz [19, 20]. Figure 6(b) shows the count rate from the SNSPD as the spectrometer wavelength is scanned across the cavity with dark counts subtracted. The time resolved measurement is performed at maximum coupling of the cavity emission.

Spontaneous emission lifetimes are measured using a time-correlated single-photon counting technique [21]. The 980 nm laser beam is chopped at 50 Hz to produce a square wave-modulated pump. The chopper provides start pulses to the time-sampling electronics, while the SNSPD provides a stop pulse each time it detects a photon. The electronics record a histogram of the number of stop counts arriving in each 20 μs time interval after a start pulse; this histogram is proportional to the time response of the PL to the square wave pump. Although the electronics record multiple stops for a single start, dead-time effects do not skew the data, given that the dead time of the electronics is 70 ns and the mean time between detected photons is typically more than 1 ms. Dark counts from the detector are measured separately and subtracted from the histogram.

Photoluminescence decay measurements performed at room temperature from the cavity resonance and unpatterned film are shown in Fig. 6(a). The initial decay is fit by a single exponential decay with time constants of 1.64 ms for unpatterned film and 1.23 ms for cavity resonant emission. We note that the PC cavity increases the PL emission rate 1.33 times. The measured total PL emission decay time (τ) from the unpatterned film is the parallel sum of radiative (τ_r) and non-radiative (τ_{nr}) decay time constants:

$$1/\tau = 1/\tau_r + 1/\tau_{nr}. \tag{1}$$

On the other hand for a cavity, the radiative decay time constant is shortened by the Purcell factor F_p, and the measured overall time constant for a cavity is:

$$1/\tau_{cav} = F_p/\tau_r + 1/\tau_{nr}. \tag{2}$$

The radiative lifetime for Er in glass hosts is typically 10 ms [14], and we expect the radiative lifetime of Er in SiN_x to be similar, as the radiative transitions originate from internally shielded 4f shell electrons and should not be host dependent. Accounting for the difference in the refractive index of SiN_x ($n = 2.1$) compared to SiO_2 ($n = 1.5$), and that the radiative lifetime in bulk material is inversely proportional to the refractive index, we estimate the radiative lifetime of Er ions in this sample to be $\tau_r = 7$ ms [22]. This is likely an underestimate of the radiative lifetime, as a total lifetime of 7 ms has been previously observed from Er in silicon nitride [23]. From the above equations, we approximate $F_p = 2.4$, which is also a conservative estimate of the Purcell enhancement if the unmodified Er radiative lifetime is greater than 7 ms.

Cryogenic-temperature photoluminescence decay measurements are shown in Fig. 6(c). The decay time constant from the unpatterned film is 3.4 ms at 3.1 K, which is two times longer than at room temperature (due to decreased non-radiative recombination) [3]. The decay rate from the PC resonator at cryogenic temperatures clearly has fast and slow decay rate components and cannot be fitted by a single exponential. A double exponential fit shown on the figure describes the data quite well. In this case, the short decay time constant is 0.5 ms and long decay time

#120921 - $15.00 USDReceived 3 Dec 2009; revised 12 Jan 2010; accepted 15 Jan 2010; published 25 Jan 2010

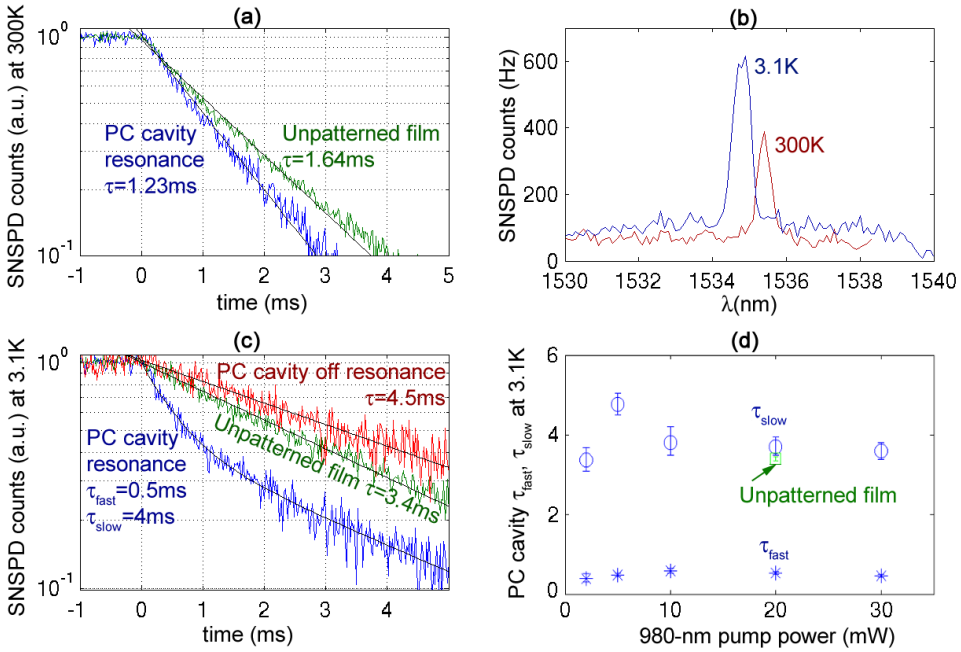

Fig. 6. (a) Time-resolved PL decay at room temperature from a PC cavity and unpatterned film. (b) Wavelength scans with SNSPD across cavity spectra measured at 300 K and 3.1 K. (c) PL decay at 3.1K from PC cavity off resonance, unpatterned film, and PC cavity resonance. (d) Time constants from bi-exponential fits to PC cavity resonance decays taken with pump powers varying from 2 mW to 30 mW.

constant is 4.0 ms, also shown in Fig. 6(d). The presence of different decay rates is expected due to two effects. First, the collected emission rate contains components coupled to the cavity mode that are enhanced and components not coupled to the cavity mode (which are not enhanced and even suppressed relative to bulk due to the presence of a photonic bandgap). Second, the Purcell enhancement of emission is position dependent as it is proportional to $|E|^2$, and the emission into the cavity mode contains components with varying emission rates. In fact, we observe 1.3-fold suppression when we look at emission decay from PC cavity off-resonance as shown in Fig. 6(c). Such a suppression of the PL decay rate originates from the reduced density of states from the 2D photonic band gap. In addition, the longer lifetime also confirms that the etching of the PC structure does not introduce surface recombination or other non-radiative decay channels that would otherwise decrease the total lifetime from the total lifetime obtained from the unpatterned region of the sample. Therefore, we can assume that the fast component of the PC cavity decay is due to an average Purcell effect, while the slow component is due to suppressed and uncoupled emission. Again, assuming that the radiative decay time constant is 7 ms for Er ions, we estimate that the average Purcell enhancement observed at 3.1 K is 11- to 17-fold. Therefore, the observed average Purcell enhancement is 5 to 7 times stronger at cryogenic temperatures than at room temperature.

Varying the pump power does not strongly affect the measured lifetimes, as shown in Fig. 6(d), which plots the time constants from bi-exponential fits to PC cavity decay rates taken at 3.1K with pump powers varying from 2 mW to 30 mW. In addtion, we find from Fig. 4(a) that the light-in/light-out characteristics do not exhibit a threshold kink. Finally, we find from Fig. 4(b) that the PC cavity Q at 5.5 K never reaches the room temperature cavity Q as pump

#120921 - $15.00 USDReceived 3 Dec 2009; revised 12 Jan 2010; accepted 15 Jan 2010; published 25 Jan 2010

power is increased, which suggests that the cavity is below transparency using the arguments of Section 5. Therefore, we confirm that it is appropriate to attribute PL decay rate enhancements measured at 20mW (Fig. 6(a),(c)) to the Purcell effect, rather than stimulated emission, which would enhance the emission rate dramatically at lasing threshold.

5. Analysis

We discuss the difference in the behavior of Qs measured for different types of cavities, at different spectral positions, and at different temperatures. Since we observe the change in Q with varying temperature and pump power in a limited spectral range around the Er absorption peak, we conclude that the observed changes in Q are mostly due to varying Er absorption. In the case of high Q, small mode volume resonators, the absorption rate is not only a property of the material, but is also affected by the cavity-modified electromagnetic environment. Namely, according to Fermi's Golden rule, stimulated emission and absorption rates depend on the same matrix elements as the spontaneous emission rate (just scaled by the number of photons), which implies that they should also be enhanced by the same (Purcell) factor F_p in cavities. Stronger Purcell enhancement for Er emission at cryogenic temperatures is expected because the Er homogeneous linewidth $\Delta\omega_{Er}$ decreases at cryogenic temperatures [3, 14]. At room temperature, $\Delta\omega_{Er}$ is greater than the cavity linewidth (bad emitter limit) and $F(T) \propto Q_{Er}/V_{mode}$, where $Q_{Er} = \omega_0/\Delta\omega_{Er}$, where ω_0 is the Er transition frequency. On the other hand, at cryogenic temperatures, $\Delta\omega_{Er}$ is expected to narrow considerably. If the Er homogeneous linewidth were comparable to or smaller than the cavity linewidth (bad cavity limit), we would have $F(T) \propto Q_{cav}/V_{mode}$ [24]. From the time resolved measurements on PC cavities, we determined that the average Purcell factor F_p is about 6 times stronger at cryogenic temperatures. Therefore, we expect that the change in average enhancement of absorption rate ($\gamma_a(T)$) by Er ions is also 6-fold as the temperature changes from 290 K to 6 K, i.e. $\gamma_a(6K) = 6 \times \gamma_a(290K)$.

For PC cavities at low pump power, the experimentally observed cavity Q (Q_{obs}) depends on the intrinsic (empty) cavity Q (Q_{cav}) and the absorption rate ($\gamma_a(T)$):

$$\frac{\omega_0}{Q_{obs}} = \frac{\omega_0}{Q_{cav}} + \gamma_a(T). \tag{3}$$

By applying the above Eq. 3 for one particular PC cavity at the main Er emission peak that has low-pump power $Q_{obs} = 16{,}000$ at 290 K and $Q_{obs} = 9{,}000$ at 6 K, we calculate $\gamma_a(290K) = 1.9 \times 10^9 Hz$ and $Q_{cav} = 19{,}000$.

For higher pump powers, Eq. 3 is no longer valid because Er ions are excited from the ground state, reducing absorption and increasing stimulated emission. At the peak of the Er emission spectrum, where the absorption and emission cross-sections are comparable, we can extend Eq. 3 to include the inversion effect as:

$$\frac{\omega_0}{Q_{obs}} = \frac{\omega_0}{Q_{cav}} + \gamma_a(T)(1 - 2\frac{Er^*}{Er}), \tag{4}$$

where Er^*/Er is the fraction of Er ions in the excited state relative to the total Er population. Equation 4 is only valid when cavities operate well below lasing threshold [25], which is again suggested by the sublinear light-in/light out characteristics. From the increase in Q_{obs} at low temperature, we can estimate Er inversion in our film. Using Eq. 4 and the calculated values for $\gamma_a(6K)$ and Q_{cav}, the observed increase of the same cavity's Q from 9,000 to 13,300 at the highest pump power in Fig. 4(a) corresponds to pumping 31% of the Er ions into excited state.

At room temperature, we would expect the PC cavity Q to increase from 16,000 at low pump power to 17,700 at high pump power if we also excite 31% of Er ions. However, experimentally we actually see a decrease in Q with pump power at room temperature in Fig. 4(b). This suggests that, at room temperature, free-carrier absorption due to the 246 nm-thick Si portion of the

#120921 - $15.00 USDReceived 3 Dec 2009; revised 12 Jan 2010; accepted 15 Jan 2010; published 25 Jan 2010

PC cavity absorbing the pump [3] or some other pump-dependent loss mechanism is stronger than the effect due to bleaching of Er absorption. If the same loss mechanism is also present at cryogenic temperatures, then 31% is an underestimate of the true percentage of excited Er ions.

In contrast to PC resonators, Er absorption inside micro-ring resonators does not change as much with temperature, as seen in Fig. 3. Since the mode volume of the micro-ring cavity is $V_{ring} = 14(\lambda/n)^3$, which is 16 times greater than the mode volume of the PC cavity, we assume that the Purcell enhancement of absorption rates is also 16 times smaller. Using these assumptions and in the same manner as for PC cavities, we find the intrinsic Q-factor $Q_{cav} = 13,300$ for the observed micro-ring WGM with measured Q-factor $Q_{obs} = 13,000$ at room temperature. The expected Q for this cavity at cryogenic temperature is 11,600, which is quite close to experimental value $Q_{obs}(6K)$=10,700.

6. Conclusion

In summary, we have shown a decrease in absorption in an Er:SiN_x system by demonstrating an increase in the cavity Q-factor with pump power in a PC cavity at cryogenic temperatures. This effect is stronger at cryogenic temperatures than at room temperature due to the large increase in the Er homogeneous linewidth with temperature. At cryogenic temperatures, PC cavities greatly enhance absorption and spontaneous emission rates as the homogeneous linewidth of Er is comparable to the cavity linewidth. From time-resolved PL measurements, we observe an increase in spontaneous emission rate in PC cavities, with an estimated Purcell enhancement of 2.4 at room temperature, and 11 to 17 at cryogenic temperatures. We also confirm that the Purcell factor enhances the coupling between Er and cavity mode by measuring weaker enhancements of absorption in large mode volume micro-ring cavities.

In the future, we hope to increase the overlap of the cavity mode and the active material, which is only 4% in the current design, through improvements in the design of the slab material. One possibility is to grow the Er-doped nitride layer in the middle of a silicon or even Si_3N_4 membrane. Removing silicon from the membrane design would also decrease absorption losses, but would increase the challenges in designing a high Q PC cavity with the low index of refraction of Si_3N_4. Removing silicon from the membrane design would also allow us to excite Er:SiN_x non-resonantly at 400 nm, where it has much higher excitation cross-section mediated by the SiN_x matrix. Despite these challenges, the demonstrated excitation of 31% of the Er ions is an important step toward realizing a laser or amplifier based on Er:SiN_x in the future.

Acknowledgment

This work was supported in part by the grants from MARCO IFC, AFOSR and the U.S. Air Force MURI program under Award No. FA9550-06-1-0470, on "Electrically-Pumped Silicon-Based Lasers for Chip-Scale Nanophotonic Systems" supervised by Dr. Gernot Pomrenke. VZ and SD acknowledge funding from NWO (VIDI grant 680-47-223). Devices were fabricated in part at the Stanford Nanofabrication Facility of NNIN supported by the National Science Foundation under Grant ECS-9731293. We would also like to acknowledge support from the Intel (MM) and the NSF (YG) fellowships. The authors would like to thank Vanessa Sih for developing the etching recipe for the PC cavities in the Er-doped silicon nitride samples, and Michel Digonnet for helpful discussions in interpreting experimental results.

#120921 - $15.00 USDReceived 3 Dec 2009; revised 12 Jan 2010; accepted 15 Jan 2010; published 25 Jan 2010